

Neutrino pair emission off electrons in a strong electromagnetic wave field

A.I. Titov^{a,b,c}, B. Kampf^{a,d}, H. Takabe^c, and A. Hosaka^e

^a*Forschungszentrum Dresden-Rossendorf, 01314 Dresden, Germany*

^b*Bogoliubov Laboratory of Theoretical Physics, JINR, Dubna 141980, Russia*

^c*Institute of Laser Engineering, Yamada-oka, Suita, Osaka 565-0871, Japan*

^d*Institut für Theoretische Physik, TU Dresden, 01062 Dresden, Germany*

^e*Research Center of Nuclear Physics,*

10-1 Mihogaoka Ibaraki, 567-0047 Osaka, Japan

Abstract

The emission of $\nu\bar{\nu}$ pairs off electrons in a polarized ultra-intense electromagnetic (e.g. laser) wave field is analyzed. We elaborate on the significance of non-linear electrodynamics effects (i.e., multi-photon processes) and the peculiarities of neutrino production. Special attention is devoted to the convergence of the reaction probabilities as a function of the number of absorbed photons. Expressions for large field intensities are provided. The asymmetry between the probabilities of electron and $\mu + \tau$ neutrino production depends on initial conditions such as energy of the wave field photons and the field intensity. These findings differ from the lowest order perturbative calculation of the reaction $\gamma + e \rightarrow e' + \nu\bar{\nu}$.

PACS numbers: 13.35.Bv, 13.40.Ks, 14.60.Ef

I. INTRODUCTION

The exact solution of Dirac's equation for an electron moving in the field of a plane electromagnetic wave was found by D. M. Volkov in 1935 [1]. The electron wave function, compared to the field-free case, changes due to a modification of its spinor structure and the appearance of an additional phase factor. The electron momentum changes to an effective quasi-momentum, and the electron mass becomes an effective "dressed" mass. These modifications depend on the dimensionless variable ξ^2 related to the amplitude of the electromagnetic four-potential A^μ [2]

$$\xi^2 = -\frac{e^2 \langle A^2 \rangle}{M_e^2}, \quad (1)$$

where e is the absolute value of electron charge ($e^2 = 4\pi\alpha$ with $\alpha \approx 1/137.035$) and M_e is the electron mass. (For a manifestly gauge invariant formulation cf. [3].)

Decades later, Volkov's solution was applied to Compton scattering [4–6] and electron-positron pair production [7] in strong electromagnetic fields. A consistent systematic analysis of these electromagnetic and further weak processes, such as pion and muon decays, $\nu\bar{\nu}$ emission by an electron in an external field etc. was performed by Nikishov and Ritus and coworkers in a series of papers [8–11] and summarized in the review [12]. Later, some aspects of weak interaction, in particular neutrino emission, by electrons in a strong electromagnetic field were considered in Refs. [13–15]. The twofold extension of QED for strong electromagnetic fields was discussed in the recent paper [16].

The main result of these previous studies is the conclusion that the quantum processes are modified significantly in strong electromagnetic fields. For instance, an electron can absorb or emit simultaneously a certain number of field photons, depending on the initial conditions of the considered process. This fact, together with the modifications of above mentioned electron properties, results in strong non-linear and non-perturbative effects which can not be described within the usual perturbative quantum electrodynamics (pQED). Consider, for example, the emission of a photon with four-momentum k' by an electron moving in a electromagnetic wave field. The process depends on the invariant variable $u = \frac{k \cdot k'}{k \cdot p}$ [2], which varies in the range of $0 < u < u_n = \frac{4nE_e\omega_L}{M_e^2(1+\xi^2)}$ for the absorption of n photons with four-momenta $k \sim (\omega_L, \mathbf{k}_L)$ by the electron with four-momenta $p \sim (E_e, \mathbf{p}_e)$ and p' prior and after the emission process. One can see that (i) the kinematical limit u_n (phase space) increases with the number of absorbed photons ("cumulative effect") and (ii) decreases with

increasing field intensity ξ^2 because of the electron mass modification. On the other hand, the contribution of higher harmonics also increases with ξ^2 , where, following [2], we use the notion "harmonics" for processes with different n 's.

Since ξ^2 plays an important role, it seems to be useful to recall the relation between ξ^2 and the electromagnetic (laser) field intensity I , where the electromagnetic field is considered as a classical background field. For the case of a monochromatic circularly polarized plane wave with four-potential $A^\mu = (0, \mathbf{A})$, where $\mathbf{A}(\phi) = \mathbf{a}_x \cos \phi + \mathbf{a}_y \sin \phi$, $\phi = k \cdot x$, and $|\mathbf{a}_x| = |\mathbf{a}_y| = a$, $\mathbf{a}_x \mathbf{a}_y = 0$, i.e. $k \cdot x = \omega_L t - \mathbf{k}_L \mathbf{x}$, the average value of A^2 is equal to $-a^2$, meaning $\xi^2 = \frac{e^2 a^2}{M_e^2}$. On the other hand, the field intensity may be expressed through the electric (\mathbf{E}) and magnetic (\mathbf{H}) field strengths by $I = \frac{c}{2}(\mathbf{E}^2 + \mathbf{H}^2) = c\mathbf{E}^2$. Taking into account $\mathbf{E} = -\partial\mathbf{A}/\partial t$, one gets an expression for the average intensity I in terms of the amplitude a , $I = ca^2\omega^2$, which leads to $\xi^2 = \frac{\alpha\hbar}{\pi(M_e c^2)^2 c} \lambda_L^2 I$, where $\lambda_L = 2\pi\hbar c/\omega_L$ is the wave length of the electromagnetic field A^μ . The dependence of ξ^2 on the electromagnetic field intensity I for different wavelengths λ_L is exhibited in Fig. 1.

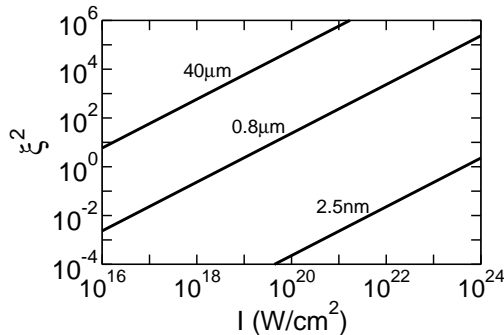


FIG. 1: Dependence of ξ^2 on the electromagnetic wave field intensity I for three values of wave length λ_L .

The wavelength $\lambda_L = 0.8 \mu\text{m}$ (or $\omega_L \simeq 1.55 \text{ eV}$) corresponds to the widely used titanium-sapphire laser oscillator (cf. Refs. [17–20]). The short wavelength $\lambda_L = 2.5 \text{ nm}$ (or $\omega_L \simeq 0.5 \text{ keV}$) corresponds to the soft x-ray (SXR) free electron laser at SLAC [21]. The long wavelength $\lambda_L = 40 \mu\text{m}$ (or $\omega_L \simeq 0.03 \text{ eV}$) may be obtained at the free electron laser for infrared experiments (FELIX) [22]. One can see that ξ^2 varies within a fairly large range, depending on the field intensity and wavelength.

In the low-frequency limit, $\omega_L \rightarrow 0$, the intensity parameter becomes large, i.e. $\xi^2 \rightarrow \infty$ at fixed intensity I or \mathbf{E} . This limit was considered in some detail by Nikishov and

Ritus [8, 9, 12] who pointed out that the invariant variable

$$\chi = \frac{e\sqrt{\langle F_{\mu\nu}p^\nu \rangle^2}}{M_e^3} = \xi \frac{k \cdot p}{M_e^2} \quad (2)$$

remains finite and the total probabilities of most of the considered processes depend only on χ [12]. Here, $F_{\mu\nu} = \partial_\nu A_\mu - \partial_\mu A_\nu$ is the electromagnetic field tensor. Such a case of simultaneous limits of $\xi \rightarrow \infty$ and $\omega_L \rightarrow 0$ at finite I corresponds to the situation of an electron interacting with a constant (crossed) electromagnetic field.

Note that two asymptotic regions of the external field were considered in most of the above quoted papers. One corresponds to the weak-field limit $\xi^2 \ll 1$. In this case, only a limited number of harmonics $n \leq 2$ contributes. The opposite case of large intensity $\xi^2 \rightarrow \infty$ with $\omega_L \rightarrow 0$ allows for two asymptotic limits: $\chi \ll 1$ and $\chi \gg 1$. Of course, such an analysis of limiting cases is interesting and important by its own. However, the rapidly evolving laser technology [23] can provide conditions where the limit of $\xi^2 \gg 1$ is achieved at finite ω_L , as well as $\chi \sim 1$ as can be inferred from Fig. 1 and by numerical evaluation of Eq. (2). Therefore, it seems relevant to consider the probabilities of quantum processes without the restrictions imposed in [12–15].

The goal of present work is accordingly an analysis of neutrino pair emission off an electron moving in a strong external electromagnetic (laser) wave field in a wide region of ξ and χ . Our paper is organized as follows. In Sect. II, we consider the neutrino pair emission. A scheme is presented to overcome convergence problems in the expansion in terms of harmonics. The employed method is similar to the one-photon emission process which is outlined in Appendix A to expose these similarities and the important differences. The perturbative neutrino pair emission is recapitulated in Appendix B. Our conclusions can be found in Sect. III.

II. EMISSION OF A NEUTRINO PAIR

A. Basic formulas

Similar to the emission of a photon by an electron moving in an electromagnetic external (background) field (see Appendix A 1) one can evaluate the emission of a neutrino pair $\nu_i \bar{\nu}_i$

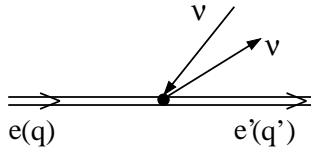


FIG. 2: Diagram for the emission of a neutrino pair off an electron in an external wave field with effective low-energy $e\bar{e}\nu\bar{\nu}$ vertex. The double lines depict electron Volkov states.

of species $i = e, \mu, \tau$ by the S matrix element

$$S_{fi}^{(i)} = -i \frac{G_F}{\sqrt{2}} \int \bar{\psi}_f^*(x) \gamma^\alpha (C_V^{(i)} - C_A^{(i)} \gamma_5) \psi_i(x) L_\alpha^{(i)} e^{iQx} \frac{d^4x}{\sqrt{2E_\nu 2E_{\bar{\nu}}}} \quad (3)$$

corresponding to the diagram in Fig. 2. M_Q is the invariant mass of the $\nu\bar{\nu}$ pair: $M_Q^2 \equiv Q^2 = (p_\nu + p_{\bar{\nu}})^2$ with $p_\nu \sim (E_\nu, \mathbf{p}_\nu)$ and $p_{\bar{\nu}} \sim (E_{\bar{\nu}}, \mathbf{p}_{\bar{\nu}})$ as four-momenta of neutrino and antineutrino. (We employ units with $\hbar = c = 1$.) The Volkov solution $\psi_i(x)$ in (3) (cf. Eq. (A2) in Appendix A 1) describes the in-state of the electron in an external wave field, while $\bar{\psi}_f^*(x)$ refers to the out-state of the electron also accounting for the external field. The neutral neutrino current

$$L_\alpha^{(i)} = \bar{u}_{\nu_i} \gamma_\alpha (1 - \gamma_5) v_{\bar{\nu}_i} , \quad (4)$$

couples directly to the electron current $\bar{\psi}_f^* \gamma^\alpha (C_V^{(i)} - C_A^{(i)} \gamma_5) \psi_i$ with a strength given by Fermi's constant $G_F = 1.66 \cdot 10^{-5} \text{ GeV}^{-2}$. The expression (3) holds in the local limit where all momenta involved in the process are much smaller than the masses of the intermediate vector bosons Z^0 and W^\pm . Then, one can obtain "universal" interactions described by the effective low-energy Lagrangian [24] for the direct current-current interaction

$$\mathcal{L}_{\text{eff}}^{(i)} = \frac{G_F}{\sqrt{2}} [\bar{u}_{\nu_i} \gamma_\alpha (1 - \gamma_5) v_{\nu_i}] [\bar{u}_e \gamma^\alpha (C_V^{(i)} - C_A^{(i)} \gamma_5) u_e] , \quad (5)$$

with

$$C_V^{(e)} = \frac{1}{2} + 2 \sin^2 \theta_W , \quad C_V^{(\mu, \tau)} = -\frac{1}{2} + 2 \sin^2 \theta_W , \quad (6)$$

$$C_A^{(e)} = \frac{1}{2} , \quad C_A^{(\mu, \tau)} = -\frac{1}{2} ; \quad (7)$$

the average value of $\sin^2 \theta_W \simeq 0.23$ is taken from Ref. [25]. In the weak-field approximation, where the interaction with the external wave field is mediated by one photon, the diagram in Fig. 2 would be resolved by diagrams exhibited in Fig. 3 corresponding to the process

$\gamma + e \rightarrow e' + \nu\bar{\nu}$ which can be dealt with perturbatively (see Appendix B). The effective weak vertices for the $e\bar{e}\nu\bar{\nu}$ interaction, in turn, are resolved in the tree-level approximation within the standard model as exhibited in Fig. 4. The advantage of the diagram in Fig. 2 and Eq. (3) is that multi-photon effects are included which become important at high intensities where the external wave behaves more and more as a classical field.

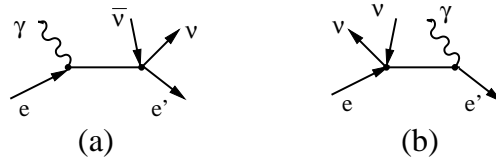


FIG. 3: Lowest order diagrams for the reaction $\gamma + e \rightarrow e' + \nu\bar{\nu}$ with effective low-energy $e\bar{e}\nu\bar{\nu}$ vertices. Diagrams (a) and (b) correspond to the direct charge and neutral vector boson exchanges.

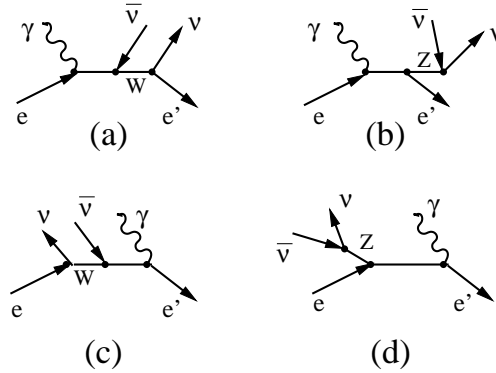


FIG. 4: Lowest order diagram for the reaction $\gamma + e \rightarrow e' + \nu\bar{\nu}$. Diagrams (a) and (b) correspond to the direct charge (neutral) vector boson exchange; (c) and (d) describe corresponding crossed channels.

As in the case of the emission of one photon (see Appendix A), the differential probability of neutrino pair emission can be represented by the infinite sum of the partial contributions,

$$dW = \sum_{n=1}^{\infty} dW^{(n)} \quad (8)$$

with

$$dW^{(n)} = \frac{G_F^2}{2(8\pi)^3} R^{(n)} \frac{du dM_Q^2 d\phi_{q'}}{q_0(1+u)^2 2\pi}, \quad (9)$$

$$R^{(n)} = \frac{8}{3} (Q_\alpha Q_\beta - g_{\alpha\beta} Q^2) \mathcal{M}_n^{\alpha\beta}, \quad (10)$$

where $\phi_{q'}$ is the azimuthal angle of the outgoing electron and

$$u = \frac{k \cdot Q}{k \cdot p'} . \quad (11)$$

Analog to the case of one-photon emission (see Appendix A 1) the label n refers to the number of photons absorbed from the external field. For the sake of simplicity, we skip henceforth the index i . The electron tensor

$$\mathcal{M}_n^{\alpha\beta} = \text{Tr}[(\not{p}' + M_e)S_n^\alpha(C_V - C_A\gamma_5)(\not{p} + M_e)S_n^\beta(C_V - C_A\gamma_5)] \quad (12)$$

incorporates the electromagnetic wave field via

$$S_n^\alpha = \left(\gamma^\alpha - \frac{M_e^2 \xi^2 k^\alpha \not{k}}{2k \cdot p k \cdot p'} \right) B_n^{(0)} + \xi M_e \left[\left(\frac{\not{\eta}_1 \not{k} \gamma^\alpha}{2k \cdot p'} + \frac{\gamma^\alpha \not{k} \not{\eta}_1}{2k \cdot p} \right) B_n^{(1)} + \left(\frac{\not{\eta}_2 \not{k} \gamma^\alpha}{2k \cdot p'} + \frac{\gamma^\alpha \not{k} \not{\eta}_2}{2k \cdot p} \right) B_n^{(2)} \right] .$$

Here, $\mathbf{n}_{1(2)}$ is the unit vector of $\mathbf{a}_{1(2)}$, and the functions B_n are related to the Bessel functions (cf. Refs. [2, 12]):

$$\begin{aligned} B_n^{(0)} &= J_n(z) e^{in\phi_{q'}} , \\ B_n^{(1)} &= \frac{1}{2} (J_{n+1} e^{i(n+1)\phi_{q'}} + J_{n-1} e^{i(n-1)\phi_{q'}}) , \\ B_n^{(2)} &= \frac{1}{2i} (J_{n+1} e^{i(n+1)\phi_{q'}} - J_{n-1} e^{i(n-1)\phi_{q'}}) . \end{aligned} \quad (13)$$

The argument of these Bessel functions is

$$z = \frac{2n\xi}{\sqrt{1+\xi^2}} \sqrt{\frac{u}{u_n} \left(1 - \frac{u}{u_n}\right) - \frac{1+u}{u_n} \frac{M_Q^2}{(1+\xi^2)M_e^2}} , \quad (14)$$

where u_n is the kinematical limit of the invariant variable u defined by

$$u_n = \frac{2n(k \cdot p)}{M_e^2(1+\xi^2)} \quad (15)$$

which determines the upper limit of M_Q^2 at given u by

$$M_{Q_{\max}}^2 = M_e^2(1+\xi^2) \frac{u(u_n - u)}{1+u} . \quad (16)$$

The functions $R^{(n)}$ in Eq. (10) do not depend on $\phi_{q'}$; the explicit expression reads

$$\frac{3}{32} R^{(n)} = C_V^2 F_V + C_A^2 F_A + 2\lambda C_V C_A F_I, \quad (17)$$

$$F_V = -M_Q^2(2M_e^2 + M_Q^2)J_n^2 + \xi^2 M_Q^2 M_E^2 \left(1 + \frac{u^2}{2(1+u)}\right) \Delta J_n^2 , \quad (18)$$

$$F_A = M_Q^2(4M_e^2 - M_Q^2)J_n^2 + \xi^2 M_E^2 \left(M_Q^2 + (M_Q^2 + 2M_e^2) \frac{u^2}{2(1+u)}\right) \Delta J_n^2 , \quad (19)$$

$$F_I = M_Q^2 M_e \frac{\xi(2+u)}{\sqrt{1+u}} \frac{\left(M_{Q_{\max}}^2 \left(1 - \frac{u_n}{2(u_n - u)}\right) - M_Q^2\right)}{\left(M_{Q_{\max}}^2 - M_Q^2\right)^{1/2}} J_n (J_{n+1} - J_{n-1}) , \quad (20)$$

where $\lambda = \pm 1$ is the relative phase (polarization) of the amplitudes \mathbf{a}_1 and \mathbf{a}_2 , and $\Delta J_n^2 = J_{n+1}^2 + J_{n-1}^2 - 2J_n^2$. Our expression coincides with the result of Ref. [15] in a different notation.

B. Numerical evaluation

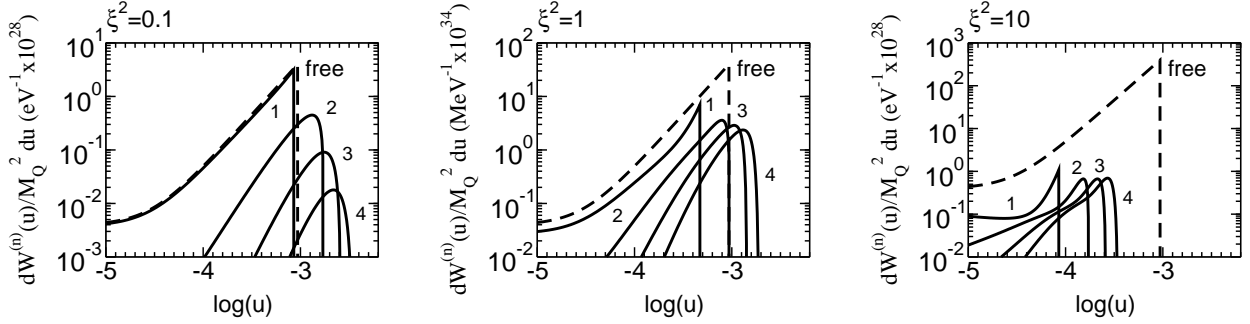


FIG. 5: Differential probability of neutrino pair emission as a function of $\log u$ for $\xi^2 = 0.1, 1$ and 10 , shown in left, middle and right panels, respectively, for the lowest harmonics $n \leq 4$. The result for the reaction $\gamma + e \rightarrow e + \nu\bar{\nu}$ calculated perturbatively (see Appendix B) is shown by the dashed curves labeled by "free". The numbers (from 1 to 4) correspond to the number of absorbed photons. The energies of the external (laser) photons and incoming electrons are chosen to be $\omega_L = 1.55$ eV and $E_e = 40$ MeV, respectively. The invariant mass of the outgoing neutrino pair is fixed at $M_Q = 10$ eV.

In Fig. 5 we exhibit the differential emission probabilities summed over all neutrino types for a head-on collision of 40 MeV electrons with a laser beam characterized by $\lambda_L = 0.8 \mu\text{m}$ (or $\omega_L \simeq 1.55$ MeV). We fix the invariant mass of the outgoing neutrino pair by $M_Q = 10$ eV. (The numerical results for the first two harmonics coincide for $\xi^2 = 0.1$ with the prediction [15] based on the asymptotic decomposition of $W(u)$ for $n = 1, 2$ in the limit $\xi^2 \ll 1$.) The prediction of perturbative QED for the reaction $\gamma + e \rightarrow e' + \nu\bar{\nu}$ (see Fig. 3 and Eq. (B5) in Appendix B) is shown by the dashed curves. One can see that for small ξ^2 the result for $n = 1$ coincides practically with that of pQED. Similar to the case of non-linear Compton scattering (see Appendix A 1), even in this case the contribution of higher harmonics increases the phase space, i.e. the kinematic limit, and modifies the total probability. When ξ^2 increases, the difference between the non-perturbative calculations and pQED is rather large, even for $n = 1$, see middle and right panels of Fig. 5.

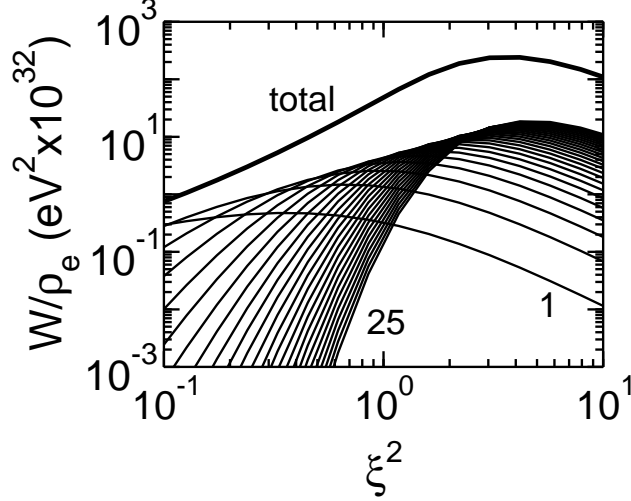


FIG. 6: The total probability of neutrino pair emission as a function of ξ^2 for the first 25 harmonics. The thick curve is their total contribution. The electron and photon energies are chosen as $E_e = 40$ MeV and $\omega_L = 1.55$ eV, respectively.

In Fig. 6 we show the total probability normalized as W/ρ_e , where ρ_e is the initial electron density divided by the electron mass in the electron rest frame,

$$\frac{1}{\rho_e}W = \sum_{n=1}^{\infty} \frac{G_F^2}{2(8\pi)^3} \int_0^{u_n} \frac{du}{(1+u)^2} \int_0^{M_Q^2 \max} dM_Q^2 R^{(n)}, \quad (21)$$

for the sum of all types of neutrinos as a function of ξ^2 for the first 25 harmonics. For small ξ^2 , $\xi^2 \leq 0.1$, along with the predominant contribution of the first two harmonics the contribution of the higher harmonics is significant. When ξ^2 increases, e.g. for $\xi^2 \simeq 10$, the contribution of higher harmonics exceeds the contribution of lowest harmonic by orders of magnitude. The qualitative difference in the relative contribution of higher harmonics to the total probability of the emission of a photon (cf. Fig. 13 in Appendix A 1) and neutrino pairs is explained by the employed four-fermion structure of the weak-interaction $e\bar{e}\nu\bar{\nu}$ vertex and the three-particle phase space. Therefore, the problem of convergence for the total probability in case of neutrino emission becomes severe and deserves special consideration.

C. Overcoming convergence problems

Figure 7 illustrates the convergence problem of the total $\nu\bar{\nu}$ emission probability with increasing ξ^2 for the case of $\omega_L = 1.55$ eV and $E_e = 40$ MeV, where the number of included harmonics goes up to $n_{\max} = 140$. One can see some saturation at $\xi^2 \leq 2$. However, for $\xi^2 > 10$ the difference of probabilities with $n_{\max} = 25$ and $n_{\max} = 140$ is more than two orders of magnitude.

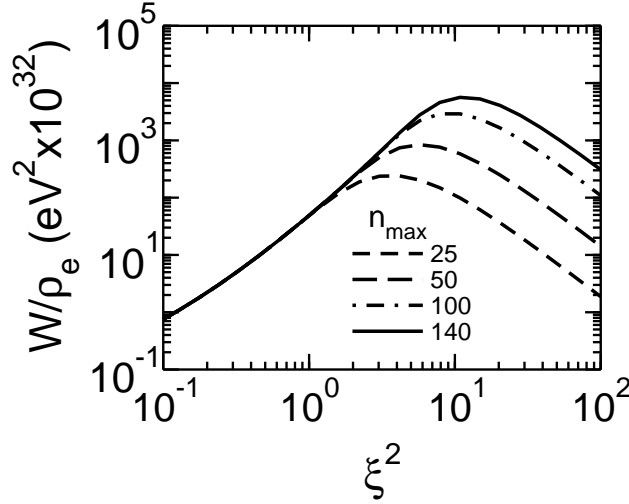


FIG. 7: The total probability of neutrino pair emission as a function of ξ^2 for different values of n_{\max} from 25 to 140. Kinematics as in Fig. 6.

The problem of convergence may be solved by the same method as proved useful for the one-photon emission (see Appendix A 1) using the transformations in Eqs. (A10) and (A11). The main difference to the one-photon emission (cf. Eq. (A13)) is a modification of the argument of the Airy functions, which emerge from the above Bessel functions, as

$$y = t \left(1 + \tau^2 + \frac{1+u}{u^2} \frac{M_Q^2}{M_e^2} \right), \quad (22)$$

and an additional integration over the invariant mass dM_Q^2 . Also, the interference term in Eq. (20) proportional to the rapidly oscillating combination $\Phi(y)\Phi'(y)$ is negligible and can be omitted. The final expression for the probability $W^{(A)}$ of $\nu\bar{\nu}$ emission in the limit of $n_{\max} \rightarrow \infty$ reads

$$W^{(A)}(\xi, \chi) = \frac{\rho_e G_F^2}{48\pi^5} \int_0^\infty \frac{\sqrt{t} du}{(1+u)^2} \int_0^\infty dM_Q^2 \int_{-\xi/2}^\infty d\tau \left(F_V^{(A)} C_V^2 + F_A^{(A)} C_A^2 \right), \quad (23)$$

$$F_V^{(A)} = -M_Q^2(2M_e^2 + M_Q^2)\Phi^2(y) + \frac{2}{t}M_Q^2M_e^2 \left(1 + \frac{u^2}{2(1+u)}\right) (y\Phi^2(y) + \Phi'^2(y)) ,$$

$$F_A^{(A)} = M_Q^2(4M_e^2 - M_Q^2)\Phi^2(y) + \frac{2}{t}M_e^2 \left(M_Q^2 + (M_Q^2 + 2M_e^2)\frac{u^2}{2(1+u)}\right) (y\Phi^2(y) + \Phi'^2(y)) ,$$

where $t = (u/2\chi)^{2/3}$.

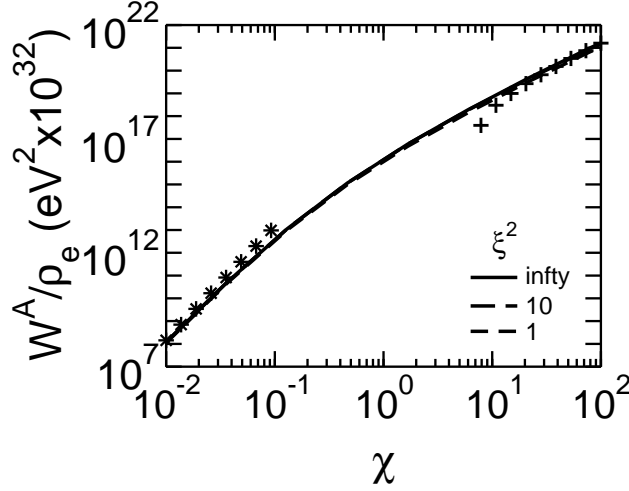


FIG. 8: The total probability $W^{(A)}(\xi, \chi)$ of neutrino pair emission as a function of χ for different values of ξ^2 as indicated in the legend. The stars and crosses correspond to the asymptotic values of $W(\infty, \chi)$ calculated by Eq. (24) for $\chi \ll 1$ and $\chi \gg 1$, respectively.

The emission probability $W^{(A)}(\xi, \chi)$ for all three types of neutrinos summed up is shown in Fig. 8 for a wide region of χ and ξ . The stars and crosses correspond to the asymptotic values of $W(\infty, \chi)$ for $\chi \ll 1$ and $\chi \gg 1$, respectively [14]:

$$W(\infty, \chi) = \begin{cases} \frac{\rho_e G_F^2 M_e^6 \chi^5}{192\sqrt{3}\pi^3} \left(\frac{49}{6}(C_V^2 + C_A^2) + 63C_A^2\right), & \chi \ll 1, \\ \frac{\rho_e G_F^2 M_e^6 \chi^2}{216\pi^3} (C_V^2 + C_A^2) \left(\ln \chi - 0.577 - \frac{1}{2} \ln 3 - \frac{5}{6}\right), & \chi \gg 1. \end{cases} \quad (24)$$

Now, the dependence $W^{(A)}(\xi, \chi)$ on ξ is weaker compared with the photon emission (cf. Fig. 15), mainly because of the additional integration over M_Q^2 . Note that the asymptotic estimates by Eq. (24) do not match in the intermediate region $0.1 \lesssim \chi \lesssim 30$.

In Fig. 9 we show the total probability $W(\xi, \chi)$ of neutrino pair emission for all neutrinos calculated for wide initial experimental conditions ranging from $\omega_L = 0.03$ eV up to

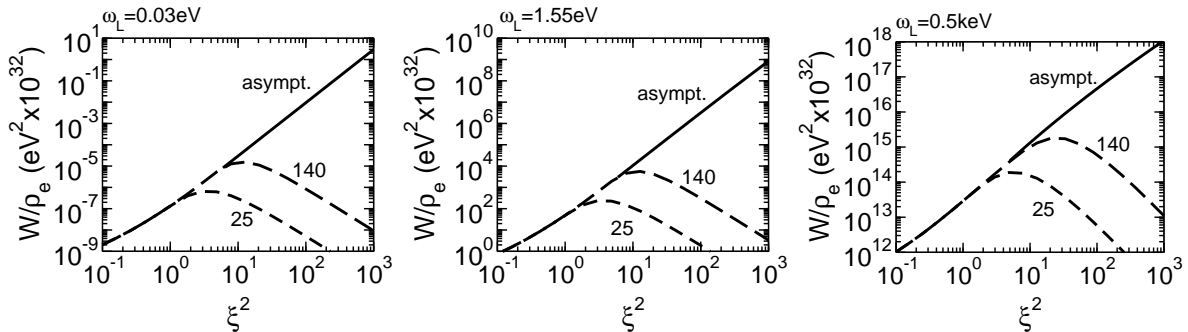


FIG. 9: The summed total probability of emission of all three types of neutrinos as a function of ξ^2 for a finite number of harmonics, $n_{\max} = 25$ and 140 (dashed curves), together with the asymptotic probability given by Eq. (23) (solid curves). The electron energy is chosen as $E_e = 40$ MeV, and the laser photon energies ω_L are 0.03 eV (left panel), 1.55 eV (middle panel) and 0.5 keV (right panel).

0.5 keV as a function of ξ^2 , where ξ^2 varies from 0.1 up to 10^3 . This interval covers possible experimental conditions illustrated in Fig. 1. At $\xi^2 > 6$, $W(\xi, \chi)$ is evaluated using the asymptotic expression of Eq. (23). For $\xi^2 \leq 6$, the probability might be evaluated as a sum of partial harmonics, in our case up to $n_{\max} = 140$. One can see that, at large ξ^2 , the difference between the probability calculated as a sum of a large but finite number of harmonics and its asymptotic value which includes an infinite number of harmonics is several orders of magnitude.

Finally, we would like to note the following. In average, the difference of neutrino pair emission probabilities for $\omega_L = 0.03$ eV and 0.5 keV is about 17 orders of magnitude (cf. left and right panels in Fig. 9). This is much greater than the corresponding difference in one-photon emission shown in the left and right panels of Fig. 16, where the corresponding difference is about 5 orders of magnitude. The difference between the two processes is explained by the different χ dependence of $W(\xi, \chi)$, shown in Figs. 8 and 15, respectively. The average values of χ for $\omega_L = 0.03$ eV and 0.5 keV are 10^{-4} and 4 , respectively. Therefore, $W(\xi, \chi)$ increases with ω_L . The sharp increase of the probability with χ in case of neutrino pair emission is a consequence of the strong energy dependence of the total probability which

can be traced back to the four-fermion structure of the $ee\nu\bar{\nu}$ matrix element.

D. Asymmetry of $\nu_e\bar{\nu}_e$ vs. $\nu_{\mu,\tau}\bar{\nu}_{\mu,\tau}$ emission

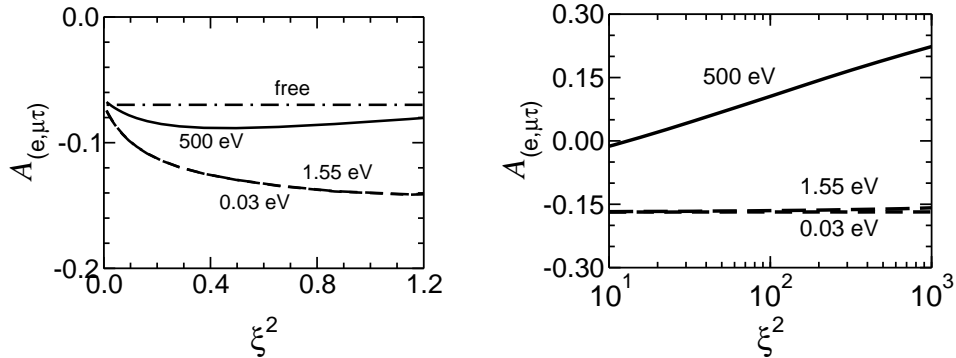


FIG. 10: Asymmetry $\mathcal{A}_{(e,\mu\tau)}$ as a function of ξ^2 for different values of the laser photon energy ω_L . Left panel: low ξ^2 ; probabilities are calculated as a sum of a finite number of harmonics according to Eq. (9). The prediction for the $\gamma + e \rightarrow e' + \nu\bar{\nu}$ reaction is shown by the dot-dashed curve labelled by "free". Right panel: high ξ^2 ; the probabilities take into account an infinite number of partial harmonics according to Eq. (23).

It seems to be interesting to analyze the asymmetry of the emission of electron and muon plus tau neutrino pairs which may be defined as

$$\mathcal{A}_{(e,\mu\tau)} = \frac{W_{(e)} - W_{(\mu+\tau)}}{W_{(e)} + W_{(\mu+\tau)}}. \quad (25)$$

Corresponding predictions for two regions of ξ^2 are shown in Fig. 10 for different values of the wave field photon energies. In the region of $\xi^2 \leq 1.2$, the probabilities are calculated as a finite sum of partial harmonics with $n_{\max} = 50$ (cf. Eq. (9)). The prediction for the $\gamma + e \rightarrow e' + \nu\bar{\nu}$ reaction (see Appendix B) is shown by the dot-dashed curve labelled by "free". Predictions for $\omega_L = 0.03$ and 1.55 eV are virtually identical. For $\xi^2 \ll 1$, all predictions are close to the results for the $\gamma + e \rightarrow e' + \nu\bar{\nu}$ reaction: $\mathcal{A}_{(e,\mu\tau)} \simeq -0.07$. All asymmetries are small in absolute value and negative, meaning a slight dominance of the emission of $\mu + \tau$ neutrinos compared to electron neutrinos.

At large ξ^2 , the probabilities are calculated as an infinite number of partial harmonics (cf. Eq. (23)). For $\omega_L = 0.03$ and 1.55 eV the range of variation of χ is $2 \cdot 10^{-5} \lesssim \chi \lesssim 3 \cdot 3 \cdot 10^{-4}$ and $1.6 \cdot 10^{-3} \lesssim \chi \lesssim 3 \cdot 1.5 \cdot 10^{-2}$, respectively. That is, the variable χ is small and

therefore, the asymmetries at these two energies are close to each other and close to the value $\mathcal{A}_{(e,\mu\tau)} \simeq -0.17$ which results from the asymptotic expression Eq. (24). For $\omega_L = 0.5$ keV and $0.34 \lesssim \chi \lesssim 4.8$ the asymmetry is positive and increases with ξ^2 . Note that, within the considered range of ξ^2 , Eq. (24) does not apply and $\mathcal{A}_{(e,\mu\tau)}$ is smaller than its asymptotic value $\simeq 0.4$ which would be found from Eq. (24). We predict a distinct dominance of emission of electron neutrino pairs compared to the sum of muon and tau neutrino pairs in the keV-range of the photon energy and at large ξ^2 . The asymmetry increases as $\ln \xi^2$ in the interval of $10 \leq \xi^2 \leq 1000$.

Finally, we note that our non-perturbative calculation of $\mathcal{A}_{(e,\mu\tau)}$ is strongly different from the prediction of pQED (cf. dot-dashed curve in the left panel of Fig. 10) in all considered intervals of ω_L and ξ^2 unless $\xi^2 \lll 1$.

III. SUMMARY

In summary we have considered $\nu_i \bar{\nu}_i$ ($i = e, \mu, \tau$) emission off an electron in a strong electromagnetic wave field in a wide range of energy of the wave field photon energy ω_L and reduced field intensity ξ^2 . Similarly to previous work we expressed the emission probability as a sum of partial harmonics, where each harmonic describes the interaction of an electron in-state with n field photons coherently. For the first time, we made a summation over harmonics up to a quite large number of harmonics and found that, at large values of field intensity, $\xi^2 > 10$, which can be achieved in current and future laser facilities, the convergence is rather weak. Therefore, we have elaborated a method allowing for a complete summation of all partial harmonics. The method is tested for one-photon emission, i.e. non-linear Compton scattering. Using this new approach we calculated neutrino pair emission in a region of ω_L and ξ^2 which can be reached experimentally in near future. We have shown that, at large ξ^2 , the difference between the finite and complete sums of partial harmonics reaches a few orders of magnitudes.

In case of neutrino pair emission we also analyzed the non-trivial asymmetry between the production of electron and $\mu + \tau$ neutrino pairs. We found that the asymmetry depends strongly on initial conditions expressed via ω_L and ξ^2 . At low ω_L , the asymmetry is negative corresponding to the dominance of emission of the $\mu + \tau$ neutrinos, while at large ω_L the asymmetry changes the sign indicating the dominance of electron neutrino pairs.

Finally, we note that all calculations (and conclusions) have been done for the sake of simplicity for the initial electron energy $E_e = 40$ MeV, which corresponds to the energy of the superconducting electron accelerator ELBE in FZ Dresden-Rossendorf [26]. One of the key variable in the considered processes, $\chi = \xi k \cdot p/M_e^2$, where k and p are the photon and electron four-momenta, respectively, directly depends on E_e . Therefore, the values of emission probabilities would also depend on E_e . The corresponding evaluation of this dependence as well as the analysis of other processes will be done in forthcoming papers. A further step towards realistic estimates is related to the inclusion of a temporal shape of the external laser wave field, as considered e.g. in [27–29].

Acknowledgments

The authors appreciate T. E. Cowan and D. Seipt for fruitful discussions.

Appendix A: Photon emission off an electron in a strong electromagnetic wave field

The methods employed in Section II are guided by the one-photon emission process off a Volkov electron, i.e. the non-linear Compton effect. To expose the similarities and differences we recall the essential steps and clarify further the notation.

1. Strong external field

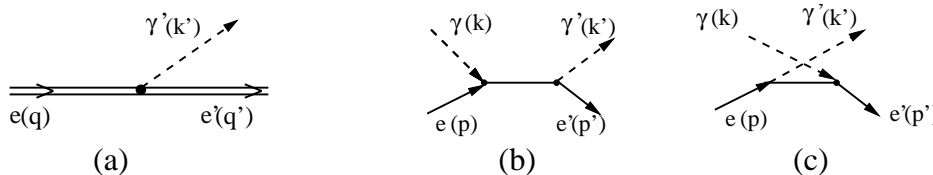


FIG. 11: (a) Diagrammatic representation of the emission of a photon off an electron in an external wave field. The double lines depict Volkov states. (b) and (c) are direct and exchange terms of the lowest-order diagrams for the perturbative treatment of the Compton process.

Let us consider the emission of a photon off an electron moving in a plane electromagnetic

wave described in the Introduction. This process is described by the S matrix element [2]

$$S_{fi} = -ie \int \bar{\psi}_f^*(\gamma \cdot \varepsilon_f^*) \psi_i e^{ik' \cdot x} \frac{d^4x}{\sqrt{2\omega'}} , \quad (\text{A1})$$

where ω' is the energy of the emitted photon with four-momentum k' and $\psi_{i(f)}$ is the electron wave function in the initial (final) state given by Volkov's solution of the Dirac equation

$$\psi_p = \left[1 + \frac{e(\gamma \cdot k)(\gamma \cdot A)}{2(k \cdot p)} \right] \exp \left[-i \int_0^{k \cdot x} \frac{e(p \cdot A)}{(k \cdot p)} d\phi' \right] \frac{u_p}{\sqrt{2q_0}} e^{-iq \cdot x} , \quad (\text{A2})$$

where γ denote Dirac matrices and q is the quasi-momentum

$$q^\mu = p^\mu - \frac{e^2 \langle A^2 \rangle}{2(k \cdot p)} k^\mu = p^\mu + \frac{e^2 a^2}{2(k \cdot p)} k^\mu = p^\mu + \frac{\xi^2 M_e^2}{2(k \cdot p)} k^\mu \quad (\text{A3})$$

of the dressed electron with effective mass

$$q^2 \equiv M_*^2 = M_e^2 \left(1 - \frac{e^2 \langle A^2 \rangle}{M_e^2} \right) = M_e^2 (1 + \xi^2) . \quad (\text{A4})$$

Note that Eq. (A1) employs the Furry picture: The field A^μ is considered as external classical (background) field, and the emission of a photon with wave four-momentum k' and polarization ε_f is described in lowest order of perturbation theory, see diagram (a) in Fig. 11.

The dependence of the potential A on $k \cdot x$ in Eq. (A2) results in the following structure of the S matrix element

$$S_{fi} = \frac{1}{\sqrt{2q_0 2q'_0 2\omega'}} \int M_{fi}(kx) e^{-i(q - q' - k') \cdot x} d^4x = \sum_{n=-\infty}^{\infty} M_{fi}^n (2\pi)^4 \delta^4(q + nk - q' - k'), \quad (\text{A5})$$

where a Fourier decomposition is used:

$$M(kx, k, k', q, q') = \sum_{n=-\infty}^{\infty} e^{-in k \cdot x} M^n(k, k', q, q') . \quad (\text{A6})$$

Thus, the amplitude is represented as a sum of an infinite number of terms which are referred to as partial harmonics. Each harmonic can be attributed to the absorption (emission) of n photons from (into) the external field A characterized by the wave four-vector k . For the photon emission off an electron the corresponding conservation law reads $q + nk = q' + k'$, cf. Eq. (A5). In case of on-shell photons, $k^2 = k'^2 = 0$ and $k' \cdot q' > 0$ hold and therefore $n \geq 1$. Correspondingly, the differential probability is the infinite sum of partial contributions:

$$dW = \sum_{n=1}^{\infty} dW^{(n)} , \quad (\text{A7})$$

where the partial harmonics $W^{(n)}$ are expressed through Bessel functions J_n of the first kind [2, 10]

$$dW^{(n)} = \frac{\alpha}{2q_0} \frac{du}{(1+u)^2} \left\{ -2J_n^2(z) + \xi^2 \left(1 + \frac{u^2}{2(1+u)}\right) (J_{n+1}^2(z) + J_{n-1}^2(z) - 2J_n^2(z)) \right\} \quad (\text{A8})$$

with

$$z = \frac{2n\xi}{\sqrt{1+\xi^2}} \sqrt{\frac{u}{u_n} \left(1 - \frac{u}{u_n}\right)}, \quad u = \frac{k \cdot k'}{k \cdot p'} = \frac{\omega'(1 - \cos\theta)}{E'_e + \omega' \cos\theta}. \quad (\text{A9})$$

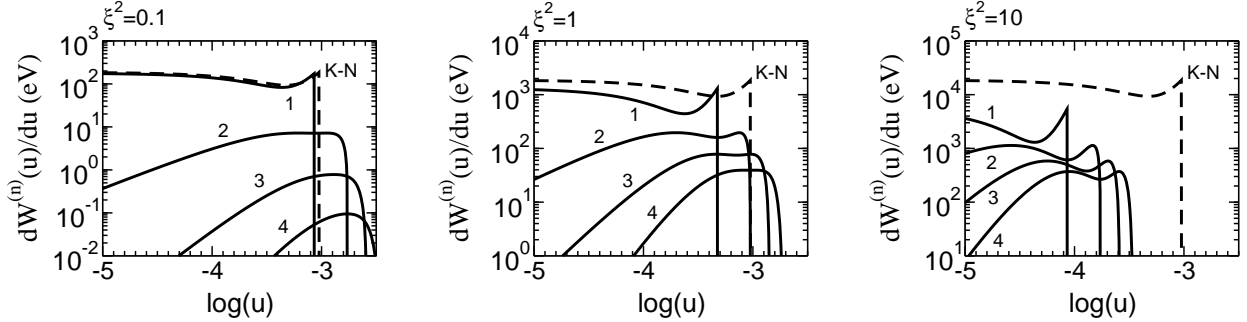


FIG. 12: Differential probability of one-photon emission as a function of $\log u$ for $\xi^2 = 0.1, 1$ and 10 , shown in left, middle and right panels, respectively, for lowest harmonics $n \leq 4$. The pQCD Compton scattering is shown by the dashed curves labelled by "K-N". The numbers (from 1 to 4) correspond to the number of absorbed photons. The energies of the laser photons and incoming electrons are chosen to be $\omega_L = 1.55$ eV and $E_e = 40$ MeV, respectively.

As an example, we exhibit in Fig. 12 the differential probabilities for photon emission by 40 MeV electrons colliding head-on with a $\lambda_L = 0.8 \mu\text{m}$ ($\omega_L \simeq 1.55$ MeV) laser beam. This process can be studied experimentally, e.g., at superconducting electron accelerator ELBE in conjunction with the 150 TW laser Draco in FZ Dresden-Rossendorf [26]. The solid curves correspond to the partial contributions which come from the coherent absorption of n photons with $n = 1 \dots 4$. The prediction of perturbative QED Compton scattering, described by the Klein-Nishina formula (see Appendix A 2), is shown by the dashed curves. One can see that for small ξ^2 , the results for $n = 1$ coincide practically with the result of pQED, cf. also [27]. However, even in this case the contribution of higher harmonics increases the phase space and modifies the total probability. When ξ^2 increases, the difference between non-perturbative calculations and pQED is rather large, even for $n = 1$. In general, the modification of the kinematical limit follows Eq. (15): u_n increases with n and decreases with ξ^2 .

In Fig. 13 we show the total probability of one-photon emission as a function of ξ^2 for the first 25 harmonics. For convenience, we show reduced probability W/ρ_e , where ρ_e is the density of initial electrons divided by the electron mass in the electron rest frame.

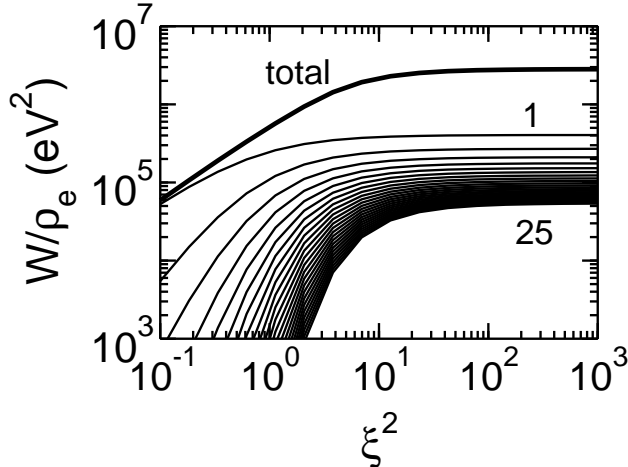


FIG. 13: The normalized probability of one-photon emission as a function of ξ^2 for the first 25 harmonics. The thick curve depicts the completely summed up result. The electron and photon energies are chosen as $E_e = 40$ MeV and $\omega_L = 1.55$ eV, respectively.

One can see that for small ξ^2 , $\xi^2 \ll 1$, the total probability is saturated by the contribution of the first two harmonics. However, at large ξ^2 , $\xi^2 \geq 10$, the contribution of higher harmonics becomes large and the convergence of the total probability as a function of the number of harmonics n is weak. Figure 14 illustrates the convergence of the emission probability with increasing ξ^2 for the case of $\omega_L = 1.55$ eV and $E_e = 40$ MeV, where the number of harmonics increases up to $n_{\max} = 140$. One can see some saturation as long as $\xi^2 \leq 10$. When ξ^2 increases, n_{\max} must further increase, in principle, as $n_{\max} \sim \xi^3$ [12].

For the calculation of the total probability for large but finite ξ^2 we use the method of Ref. [12] based on utilizing the properties of the Bessel functions $J_n(z)$ at large values of n and z and replacing the sum of n contributions by an integral over n . Ultimately, this procedure reduces to the following transformations

$$J_n^2(z) \rightarrow \frac{1}{\pi^2 \xi^2 t} \Phi^2(y), \quad (\text{A10})$$

$$J_{n+1}^2(z) + J_{n-1}^2(z) - 2J_n^2(z) \rightarrow \frac{2}{\pi^2 \xi^4 t^2} \left(y \Phi^2(y) - \Phi'^2(y) \right), \quad (\text{A11})$$

$$dn = \frac{u}{\chi} \xi^2 d\tau, \quad -\frac{\xi}{2} \geq \tau < \infty, \quad (\text{A12})$$

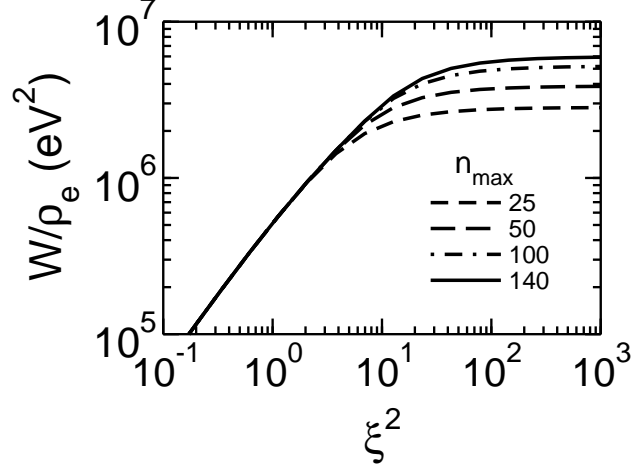


FIG. 14: The normalized total probability of one-photon emission as a function of ξ^2 for different values of n_{max} from 25 to 140 as indicated in the legend. Kinematics as in Fig. 13.

where $\Phi(y)$ is the Airy function, and

$$t = (u/2\chi)^{2/3}, \quad y = t(1 + \tau^2), \quad \chi = \xi \frac{kp}{M_e^2}. \quad (\text{A13})$$

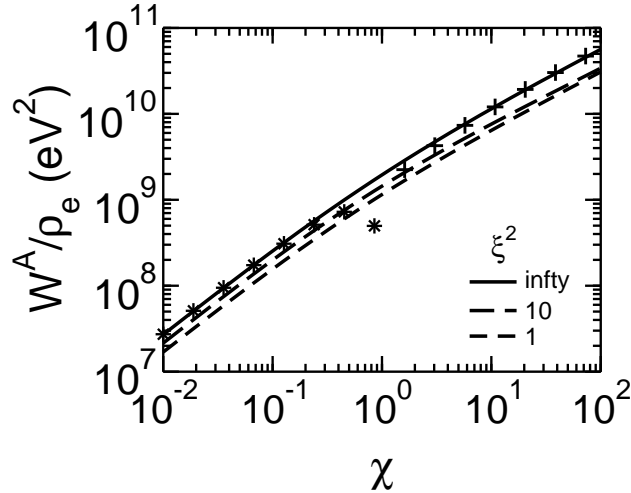


FIG. 15: The normalized total probability of one-photon emission $W(\xi, \chi)$ as a function of χ for different values of ξ^2 as indicated in the legend. The crosses and stars correspond to the asymptotic values of $W(\infty, \chi)$ for $\chi \gg 1$ and $\chi \ll 1$, respectively.

The corresponding probability is expressed in the following form:

$$W(\xi, \chi) = \frac{\rho_e \alpha M_e^2}{\pi^2} \int_0^\infty \frac{\sqrt{t} du}{(1+u)^2} \int_{-\xi/2}^\infty d\tau \left[-\Phi^2(y) + \left[1 + \frac{u^2}{2(1+u)}\right] \frac{1}{t} \left(y\Phi^2(y) - \Phi'^2(y) \right) \right]. \quad (\text{A14})$$

Contrary to Ref. [12] and related papers we do not put $\xi \rightarrow \infty$ in the above integral, which allows to calculate the probabilities at large but finite values of ξ^2 in a wide range of χ . In Fig. 15 we show $W(\xi, \chi)$ as a function of χ for different values of ξ^2 . The crosses and stars correspond to the asymptotic values of $W(\infty, \chi)$ at $\chi \gg 1$ and $\chi \ll 1$, respectively [12]:

$$W(\infty, \chi) = \begin{cases} \frac{5\rho_e \alpha M_e^2}{2\sqrt{3}} \left(1 - \frac{8\sqrt{3}}{15}\chi + \frac{7}{2}\chi^2 + \dots \right), & \chi \ll 1, \\ \frac{14\rho_e \alpha M_e^2}{27} \Gamma\left(\frac{2}{3}\right) (3\chi^{2/3}) \left(1 - \frac{45}{28} \frac{1}{\Gamma\left(\frac{2}{3}\right)(3\chi^{2/3}) + \dots} \right), & \chi \gg 1. \end{cases} \quad (\text{A15})$$

In Fig. 16 we show the total probability $W(\xi, \chi)$ calculated for a wide region of possible experimental conditions ranging from a photon energy of $\omega_L = 0.03$ eV up $\omega_L = 0.5$ keV as a function of ξ^2 , for ξ^2 varying from 0.1 up to 10^4 . This interval covers possible experimental conditions illustrated in Fig. 1. For $\xi^2 > 10$, $W(\xi, \chi)$ is evaluated using the asymptotic expression of Eq. (A14). For $\xi^2 \leq 10$, the probability is calculated as a sum of partial harmonics, in our case up to $n_{\text{max}} = 140$. At the matching point $\xi^2 = 10$, the difference between the two expressions is less than 5%.

2. Perturbative treatment

To prove the equivalence of the probabilities defined above to usual partial cross sections we recollect here also the perturbative treatment of the scattering of a photon off an electron (Compton scattering, see middle and right panels in Fig. 11). The cross section reads in standard notation

$$d\sigma^{\gamma+e' \rightarrow \gamma'+e} = \frac{1}{16\pi(s - M_e^2)} |T_{fi}|^2 dt, \quad (\text{A16})$$

where $s = (p + k)^2$ is the square of total energy and $t = (k - k')^2$ denotes the square of the momentum transfer. T_{fi} is the invariant amplitude which consists of direct and crossed terms, schematically depicted in Fig. 11 (b) and (c), respectively,

$$T_{fi} = e^2 \epsilon_\mu^*(\gamma') \epsilon_\nu(\gamma) [\bar{u}(p') M^{\mu\nu} u(p)], \quad (\text{A17})$$

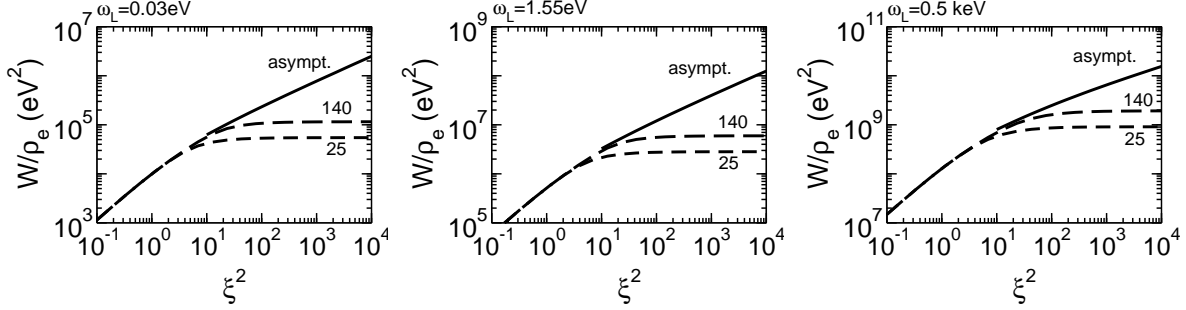


FIG. 16: The normalized total probability of one-photon emission as a function of ξ^2 for all harmonics summed (solid curves) compared to the summed contributions of the first 25 and 140 harmonics (dashed curves) with the asymptotic probability given by Eq. (A14). The electron energy is chosen as $E_e = 40$ MeV, and the photon energies ω_L are 0.03 eV (left panel), 1.55 eV (middle panel) 0.5 keV (right panel).

where $\epsilon(\gamma)$ and $\epsilon(\gamma')$ denote the polarization vectors of incoming (γ) and outgoing (γ') photons, respectively, $u(p)$ and $u(p')$ are Dirac spinors of incoming and outgoing electrons, normalized as $\bar{u}u = 2M_e$, and $M^{\mu\nu}$ is the transition operator

$$M^{\mu\nu} = \gamma^\mu \frac{\gamma \cdot p + \gamma \cdot k + M_e}{2p \cdot k} \gamma^\nu + \gamma^\nu \frac{\gamma \cdot k - \gamma \cdot p' + M_e}{2p' \cdot k} \gamma^\mu. \quad (\text{A18})$$

In Eq. (A16) averaging over the initial and summation over the final spin states are provided. The corresponding calculation is described in text books (for example in [2]). The result is the Klein-Nishina formula

$$\frac{d\sigma}{dt} = \frac{\pi r_0^2 M_e^2}{(s - M_e^2)^2} F(p, p', k), \quad (\text{A19})$$

where $r_0 \equiv \alpha/M_e$ is the "classical" electron radius and

$$F(p, p', k) = \left\{ \left(\frac{M_e^2}{2k \cdot p} + \frac{M_e^2}{2k \cdot p'} \right)^2 + \left(\frac{M_e^2}{2k \cdot p} + \frac{M_e^2}{2k \cdot p'} \right) - \frac{1}{4} \left(\frac{k \cdot p}{k \cdot p'} + \frac{k \cdot p'}{k \cdot p} \right) \right\}. \quad (\text{A20})$$

For the further analysis it is convenient to use the invariant variables $u = \frac{k \cdot k'}{k \cdot p'}$ and $dt = 2k \cdot p du / (1 + u)^2$ and to employ the probability dW of the $\gamma + e \rightarrow \gamma' + e'$ reaction, instead of the cross section $d\sigma$,

$$dW = \frac{2s\rho_\gamma}{s + M_e^2} d\sigma, \quad (\text{A21})$$

where ρ_γ is the photon density (or inverse volume per one photon), defined similarly to the dependance of ξ^2 on I mentioned in the Introduction,

$$\rho_\gamma = \frac{s - M_e^2}{2\sqrt{s}} \frac{M_e^2 \xi^2}{4\pi\alpha}. \quad (\text{A22})$$

Inspection of Eqs. (A19), (A21) and (A22) shows that Compton scattering is independent of ξ^2 . Variation of ξ^2 (or field intensity I) changes the density of photons ρ_γ , and therefore only determines the overall normalization of dW .

Appendix B: Perturbative treatment of neutrino pair emission

Consider first neutrino pair production in the reaction $\gamma + e \rightarrow e' + \nu_i \bar{\nu}_i$. The differential cross section reads

$$\frac{d\sigma^{(i)}}{dM_Q^2 du} = \frac{2}{(8\pi)^3 (s - M_e^2) (1 + u)^2} \int \frac{d\Omega_\nu}{4\pi} |T^{(i)}|^2, \quad (\text{B1})$$

where Ω_ν is the solid angle of outgoing neutrino in the $\nu\bar{\nu}$ rest frame. The invariant amplitude $T^{(i)}$ in lowest order (tree level) of the Glashow-Salam-Weinberg model is described by the Feynman diagrams depicted in Fig. 4. Accordingly, the electron neutrino pairs are produced via exchange of both the charged W^\pm and neutral Z^0 vector bosons, while the muon and tau neutrino pairs are produced only through the neutral boson exchange when assuming individual lepton number conservation. In the local limit, where all the momenta involved in the process are much smaller than the masses of the intermediate vector bosons, by making use of a Fierz transformation for the charged boson exchange, one can obtain "universal" effective interactions depicted in Fig. 3 as direct (a) and exchange (b) terms. This interaction is described by the effective Lagrangian in Eq. (5). Then, the invariant amplitude is expressed as

$$T^{(i)} = \frac{eG_F}{\sqrt{2}} L_\alpha^{(i)} \epsilon_\beta(\gamma) \cdot [\bar{u}(p') M^{(i)\alpha\beta} u(p)], \quad (\text{B2})$$

where $L_\alpha^{(i)}$ is defined by Eq. (4), and the transition operator $M^{(i)\mu\nu}$ is defined by Eq. (A18) with the substitution

$$\gamma^\mu \rightarrow \gamma^\mu (C_V^{(i)} - C_A^{(i)} \gamma_5). \quad (\text{B3})$$

Summation over spins of the neutrinos (with the assumption $m_\nu = 0$) and integration over the solid angle in Eq. (B1) leads to

$$\int \frac{d\Omega_\nu}{4\pi} \text{Tr}[L_\alpha L_\beta^\dagger] = \frac{8}{3}(Q_\alpha Q_\beta - g_{\alpha\beta} Q^2), \quad (\text{B4})$$

and one can rewrite Eq. (B1) as

$$\frac{d\sigma^{(i)}}{dM_Q^2 du} = \frac{\alpha G_F^2}{512\pi^2(s - M_e^2)(1 + u)^2} F^{(i)}(p, p', k, Q^2), \quad (\text{B5})$$

$$F^{(i)}(p, p', k, Q^2) = \frac{8}{3}(g^{\alpha\beta} Q^2 - Q^\alpha Q^\beta) g^{\nu\nu'} \text{Tr}[M_{\alpha\nu}^{(i)} M_{\beta\nu'}^{(i)\dagger}]. \quad (\text{B6})$$

-
- [1] D. M. Volkov, *Z. Phys.* **94**, 250 (1935)
 - [2] V. B. Berestetskii, E. M. Lifshitz, and L. P. Pitaevskii, *Quantum Electrodynamics*. 2nd ed., (Course of theoretical physics; vol. 4), Pergamon Press Ltd. (1982).
 - [3] T. Heinzl and A. Ilderton, *Opt. Commun.* **282**, 1879 (2009).
 - [4] N. D. Sengupta, *Bull. Calcutta Math. Soc.* **44**, 175, (1952).
 - [5] I. I. Goldman, *Phys. Lett.* **8**, 103 (1964)
 - [6] L. S. Brown and T. W. B. Klibbe, *Phys. Rev. A* **133**, 705 (1964).
 - [7] H. R. Reiss, *J. Math. Phys.* **3**, 59 (1962).
 - [8] A. I. Nikishov and V. I. Ritus, *Sov. Phys. JETP* **19**, 529 (1964) [*Zh. Eksp. Teor. Fiz.* **46**, 776 (1964)].
 - [9] A. I. Nikishov and V. I. Ritus, *Sov. Phys. JETP* **19**, 1191 (1964) [*Zh. Eksp. Teor. Fiz.* **46**, 1768 (1964)];
V. I. Ritus, *Sov. Phys. JETP* **29**, 532 (1969) [*Zh. Eksp. Teor. Fiz.* **56**, 986 (1969)].
 - [10] N. B. Narozhnyi, A. I. Nikishov, and V. I. Ritus, *Sov. Phys. JETP* **20**, 622 (1965) [*Zh. Eksp. Teor. Fiz.* **47**, 930 (1964)].
 - [11] A. I. Nikishov and V. I. Ritus, *Sov. Phys. JETP* **25**, 1135 (1967) [*Zh. Eksp. Teor. Fiz.* **52**, 1707 (1967)].
 - [12] V. I. Ritus, *Tr. Fiz. Inst. Akad. Nauk SSSR*, **111**, 152 (1979) [*Proc. P. N. Lebedev Phys. Inst. Acad. Sci. USSR* **111** (1979)].
 - [13] V. A. Lyulka, *Zh. Eksp. Teor. Fiz.* **69**, 800 (1975).
 - [14] N. P. Merenkov, *Yad. Fiz.* **42**, 1484 (1985).

- [15] V. V. Skobelev, *Yad. Fiz.* **46**, 1738 (1987).
- [16] T. Heinzl, A. Ilderton, and M. Marklund, *Phys. Rev. D* **81**, 051902 (2010).
- [17] W. P. Leemans *et al.*, *Nature Physics* **2**, 696 (2006);
K. Nakamura *et al.*, *Phys. Plasmas* **14**, 056708 (2007).
- [18] A. Henig *et al.*, *Phys. Rev. Lett.* **102**, 095002 (2009).
- [19] J. Faure, C. Rechatin, A. Norlin, A. Lifschitz, Y. Glinec, and V. Malka, *Nature* **444**, 737 (2006).
- [20] S. P. D. Mangles *et al.*, *Nature* **431**, 535 (2004).
- [21] https://slacportal.slac.stanford.edu/sites/lcls_public/Instruments/SXR/Pages/default.aspx
- [22] <http://www.rijnh.nl/felix/>
- [23] G. A. Mourou, T. Tajima, and S. V. Bulanov, *Rev. Mod. Phys.* **78**, 309 (2006);
Y. I. Salamin, S. X. Hu, K. Z. Hatsagortsyan, and C. H. Keitel, *Phys. Rep.* **427**, 41 (2006);
M. Marklund and P. K. Shukla, *Rev. Mod. Phys.* **78**, 309 (2006);
G. Gregori *et al.*, *High Energy Density Phys.* **6**, 166 (2010).
- [24] L. B. Okun, *Leptons and Quarks, Amsterdam, Netherlands: North-holland (1982)*.
- [25] K. Nakamura *et al.* (Particle Data Group), *J. Phys. G* **37**, 075021 (2010).
- [26] <http://www.fzd.de/db/Cms?pNid=132>
- [27] D. Seipt and B. Kämpfer, arXiv:1010.3301 [hep-ph].
- [28] T. Heinzl, D. Seipt, and B. Kämpfer, *Phys. Rev. A* **81**, 022125 (2010);
C. Harvey, T. Heinzl, and A. Ilderton, *Phys. Rev. A* **79**, 063407 (2009).
- [29] N. B. Narozhny, S. S. Bulanov, V. D. Mur and V. S. Popov, *Phys. Lett. A* **330**, 1 (2004).